SAND2017-7975J

# Evaluating the Coda Phase Delay Method for Determining Temperature Ratios in Windy Environments

Sarah Albert[1], Daniel Bowman[1], Arthur Rodgers[2], and Douglas Seastrand[3]

[1]Sandia National Laboratories, Albuquerque, NM 87123

[2]Lawrence Livermore National Laboratory, Livermore, CA 94551

[3]National Security Technologies, North Las Vegas, NV 89030

## Abstract

We evaluate the acoustic coda phase delay method for estimating changes in atmospheric phenomena in realistic environments. Previous studies verifying the method took place in an environment with negligible wind. The equation for effective sound speed, which the method is based upon, shows that the influence of wind is equal to the square of temperature. Under normal conditions, wind is significant and therefore cannot be ignored. Results from this study confirm the previous statement. The acoustic coda phase delay method breaks down in non-ideal environments, namely those where wind speed and direction varies across small distances. We suggest that future studies make use of gradiometry to better understand the effect of wind on the acoustic coda and subsequent phase delays.

## I. INTRODUCTION

A series of low amplitude arrivals often follow the passage of an impulsive pressure wave. This is known as the acoustic coda, and is generated via wave interaction with topography and local atmospheric structure. Assuming that the acoustic source and receiver remain in the same location, acoustic coda variation between successive events implies a change in the atmosphere. Thus, we can solve for localized atmospheric variation by utilizing a series of explosions at a common location and recorded along common paths.

The seismic equivalent of the acoustic coda was first identified as signal by Aki and Chouet in 1975[1]. Since then, the seismic coda has been identified as a useful tool for understanding seismic wave propagation. For example, seismic codas have been used to detect small changes in the medium through which waves travel[8], to model phase delays from changes in crustal velocities[5], to estimate attenuation[7], and to determine velocity change in a magma chamber[6]. Acoustic codas, however, have only recently been used to estimate temperature change over time[3] and velocity differences in the nocturnal boundary layer[4,2]. Previous research by Marcillo *et al.* (2014)[3] uses acoustic coda phase delays to estimate changes in temperature between a series of explosions. The results in the original study are promising, but were completed in an environment with negligible wind. Therefore, we test the limits of the method by transferring it to a non-ideal environment: one with spatially varying wind speed and direction.

## II. EXPERIMENTATION SETUP

Our experimentation setup consisted of a series of four above-ground chemical explosions on the Nevada National Security Site (NNSS). The events ranged in size from 87 – 1000kg TNT equivalent and were placed either at or above the ground surface (Table 2).

| Event # | Height Above Ground (m) | Size (kg TNT equivalent) |
|---|---|---|
| 1 | 0 | 87 |
| 2 | 2 | 87 |
| 3 | 2 | 100 |
| 4 | 0 | 1000 |

Table 1: Height above ground and size of each event in this study.

Twenty-three infrasound sensors collected the acoustic data for this study. Sensors were placed at various azimuths and ranges from ground zero (Figure 1). There were two main lines of sensors as well as a number of sensors encircling ground zero. Ten sensors were placed in a line trending S–SE, while six were placed over complex topography in a line trending to the SW. The remaining seven sensors were placed 100 – 200m in all directions around ground zero. The acoustic data was complimented by a robust meteorological dataset consisting of ground weather stations, a radiosonde deployment, and wind light detection and ranging (LIDAR). For the purposes of this study we focus on data from the

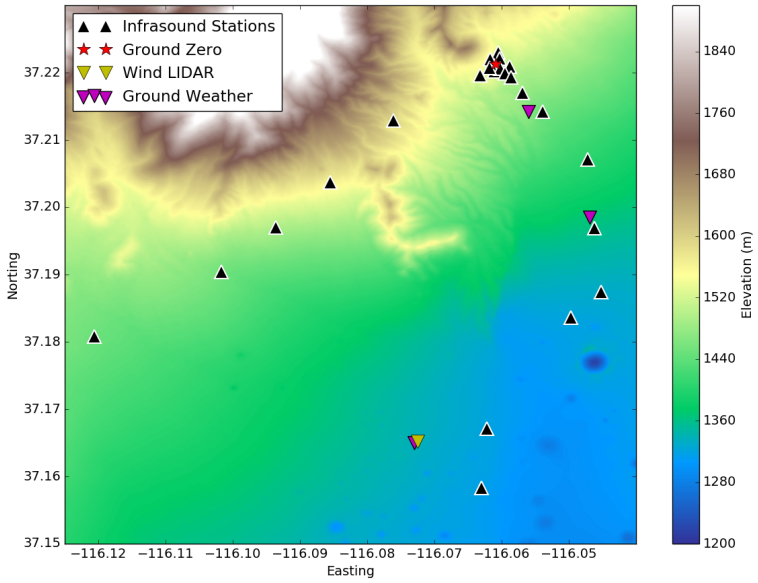


Figure 1: Infrasound sensor, ground weather, and wind LIDAR stations surrounding ground zero at the study site.

ground weather stations and wind LIDAR. The robust meteorological dataset created a unique opportunity to compare derived atmospheric phenomena with direct observations.

## III. METHOD

The availability of acoustic and meteorological data allowed us to test the limits of the method of using acoustic coda phase delays to determine changes in air temperature between events[3]. Marcillo *et al.*[3] effectively used this method on an experiment that required low wind for event detonation and occurred in a rugged canyon environment well-suited for acoustic coda scattering. Theoretically, the method should be transferrable to environments with spatially consistent wind as this would have the same effect

throughout the network. Our experiment had liberal constraints for source execution, creating an opportunity to test the method in non-ideal conditions.

Prior to estimating temperature change the acoustic coda must first be extracted at each sensor for each event. First, we imported waveforms from each sensor within a 60 minute window around the event time. A 60 minute window was chosen for ease of import, knowing that the signal of interest would be the highest amplitude within that range. The coda was extracted between 0.2 – 4.2 seconds after the peak amplitude. 0.2 and 4.2 seconds post-peak was chosen for the beginning and end of the coda, respectively, by an analyst. This value is reasonable considering the frequency content of the event signals.

After extracting the acoustic coda for each event, cross correlograms were created for all signals. Each cross correlogram is a product of computing the cross correlation values between codas from different events at the same sensor. To create each cross correlogram, correlations were calculated in 0.1 second increments with 50% overlap. In order to identify features that correspond to scatterers, changes in air temperature, and changes in wind direction each correlation window is plotted in succession. Marcillo *et al.* (2014)[3] explain that features from scatterers are identifiable by their consistent presence in the cross correlograms for multiple event pairs. Features that correspond to the main trend of the cross correlograms, or the trend of the highest cross correlation coefficients in each window, are due to changes in temperature. The third type of feature is variable between events

and results from changes in wind speed and direction.

For this method we focus on the second feature, the main trend of the highest cross correlation coefficients, which is used in the calculation for temperature ratio. We begin with the equation for effective sound speed, $c_{eff} = c + \vec{n} \cdot \vec{w}$ where $T$ is temperature in Kelvin, $c = c(T) \cong 20.06\sqrt{T}$ and corresponds to adiabatic sound speed, $\vec{n}$ is the vector normal to the direction of propagation, and $\vec{w}$ is the wind vector. It is important to note that in this equation temperature is a scalar and wind is a vector. Solving for a scalar, and thus temperature, is straightforward while solving for a vector, like wind, is more difficult. To complicate matters, the effective sound speed equation shows that only the square root of an increase in temperature effects sound speed while the entire wind vector has an effect. Consequently, wind has a larger influence on effective sound speed.

Since the geometry of events, sensors, and path effects (topography and other scatterers) remains the same, we can implement the following equation from Marcillo *et al.* (2014) to find changes in air temperature between events[3]:

$$\frac{T_1}{T_2} = \left(1 + \frac{\delta t^i}{t_1^n}\right)^2 \tag{1}$$

where $\delta t^i$ is the phase delay and $t_1^n$ is the arrival time of the signal scattered by the $n^{th}$ element. $\frac{\delta t^i}{t_1^n}$ can be found by the slope of the best fit line of the maximum values in each window of the cross correlogram (feature 2 from above). A sample cross correlogram along

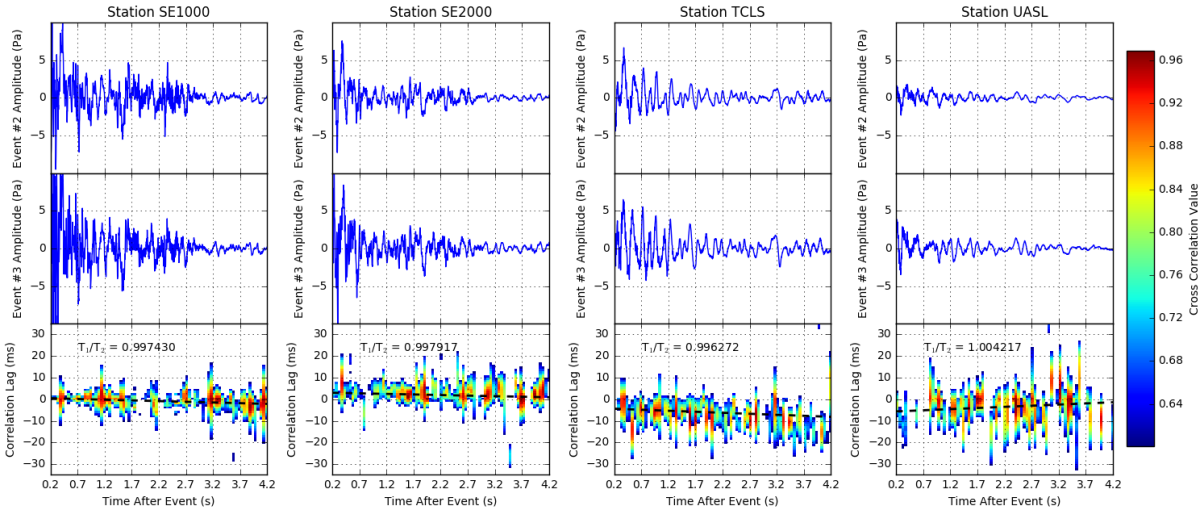


Figure 2: Sample cross corellogram at various sensors comparing events 2 and 3. Here, only cross correlations greater than 0.7 are displayed in each correlation window. The best fit line to the maximum correlation values in each window is shown by the black line. The slope of this line is used in the calculation of temperature ratio.

with its best fit line to the correlation maxima is shown in Figure 2.

Fitting a line to the correlation maxima is an important step in the calculation of temperature ratio. In our case, some correlation windows showed low values. Therefore, we chose to calculate the best fit line using linear least squares regression and weighting each point based on the standard deviation of its corresponding correlation window. The individual uncertainties in temperature ratio calculations, plotted later in this text, were calculated in the same fashion.

## IV. RESULTS

Presented here is the comparison between the second and third events, as those were the same height above ground and about the same size. However, all event pairs yielded similar results. First, temperature ratios are plotted against elevation, distance from the source, and back-azimuth to the source (Figure 3). Uncertainty estimates for each temperature ratio are included to show variance. Temperature ratios at each sensor are also plotted upon topography to show possible trends in temperature ratio with regard to elevation, distance, and back-azimuth (Figure 4). Note that in either case the temperature ratios differ at each station. Apart from that, there seems to be no obvious clustering of temperatures in any plot. Changes in temperature ratio are summarized in Table 2.

As described previously, the experiment was accompanied by a robust meteorological dataset. Due to atmospheric conditions at the site (low particulates, dry air) the wind LIDAR system could only measure winds up to 300m. This is low for the system, but adequate for our purposes because it captures the direct wave path being measured. Wind LIDAR shows that during the second event the winds were quite variable in time, but during the third event they were mostly in the N–NE direction (Figure 5). Winds recorded near the ground surface (0 – 70m) are unreliable as the purpose of the system is largely to gather wind information higher in the atmosphere (above 100m and up to a few km).

Six ground weather stations were deployed during the experiment. We choose to focus

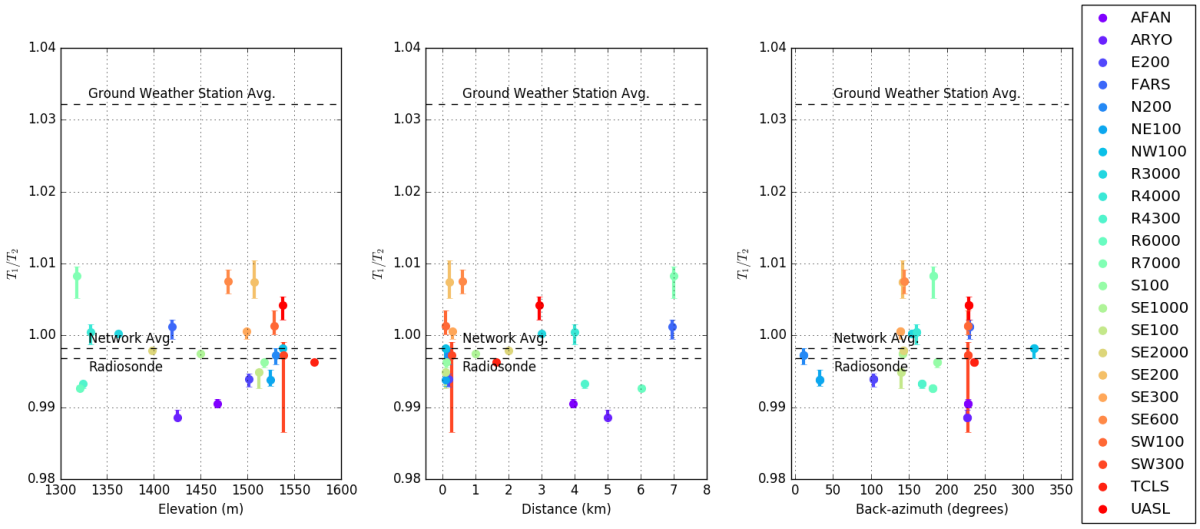


Figure 3: Temperature ratios estimated by comparing acoustic coda from events 2 and 3. Error bars represent the standard deviation in the cross correlogram used to estimate temperature ratios. Ratios are plotted against elevation, distance, and back-azimuth to help identify trends in the results. Temperature ratio observations from ground weather stations, a radiosonde, and the network average are plotted as black dashed lines for reference.

on the closest three ground weather stations as these lay within our infrasound network. Figure 4 shows winds recorded at ground stations during each event. Changes in wind speed and direction are summarized in Table 2. Note that for each event wind speed and direction varies spatially at about 1km distances. Variable winds at the ground level present a problem for our analysis because, as described by the equation for effective sound speed, changes in wind have a greater effect than changes in temperature. Fitting a line to phase delays is the backbone of this method and variable winds across the site ultimately

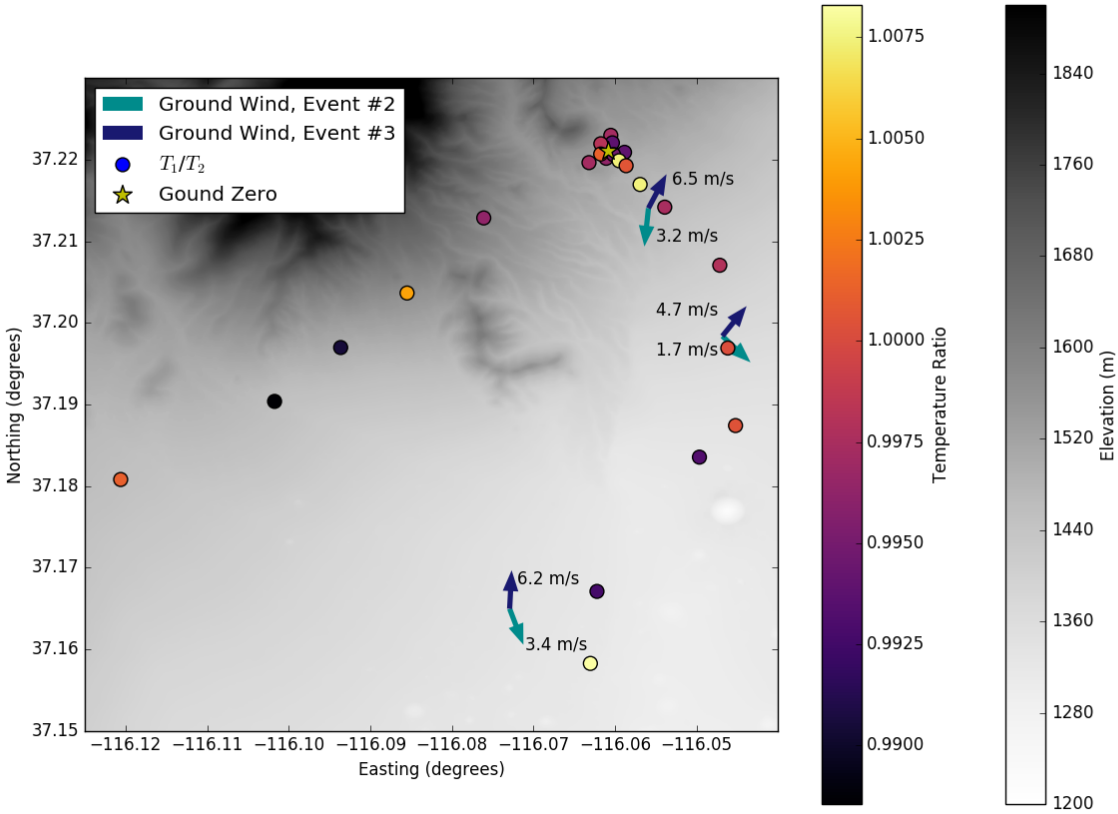


Figure 4: Temperature ratios plotted against flattened topography. Each point corresponds to a sensor location, while its color represents the temperature ratio calculated at that sensor. There are no obvious trends in temperature ratio values. Wind speed and direction for events 2 and 3 are shown by turquoise and blue arrows, respectively. Note that ground winds vary substantially across the site.

120 change phase delays. Therefore, the resulting slope of the best fit line will thus vary across
121 the site.

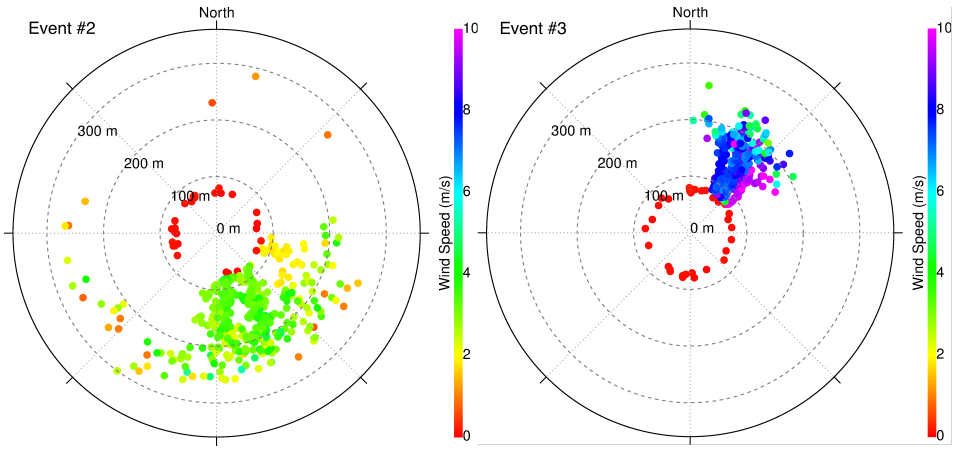


Figure 5: Wind LIDAR measurements during events 2 and 3. Note that winds were variable with altitude during event 2, but more consistently to the N–NE during event 3. Due to atmospheric conditions at the time, measurement could not be taken above 300m altitude. The nature of the instrument results in measurements near ground level (0 – 70m) that are unreliable.

| Radiosonde $T_1/T_2$ | Network Avg. $T_1/T_2$ | $\Delta$ Wind Speed | $\Delta$ Wind Direction |
|---|---|---|---|
| 0.997 | 0.998 | 2.8 – 3.3 m/s | 94 – 158 degrees |

Table 2: Height above ground and size of each event in this study.

122 ## V. DISCUSSION

123 Based on the method by Marcillo *et al.* (2014)[3], we expected either to see only small
124 deviations or clustering in temperature ratio in regions across the site. This is not the case.

It is evident that phase delays from varying wind speed and direction complicate our results. At our site, the wind is not steady in space, and likely not in time either. If the wind were consistent over the entire network, the method proposed by Marcillo *et al.* (2014)[3] would return temperature ratios that match those observed in meteorological data. Upon comparison, individual calculated temperature ratios do not match meteorological observations and meteorological observations show variance. However, the network average temperature ratio does match the radiosonde temperature ratio.

This method was proven in a flat environment with negligible wind[3]. In contrast, our winds were 1.7 – 6.5 m/s and variable. There is significant topography at our site, but it is unlikely this has an effect on the complexity in our results since the source-scatterer-receiver geometry remains the same for each event. Therefore, our results show that this method breaks down in complex wind patterns (i.e. variance in speed and direction over small scales).

## VI. CONCLUSIONS

### A. Complexities in Temperature Ratio

The method used in this study was previously validated under low wind conditions. However, in complex wind environments the method breaks down. Simply stated, one cannot ignore local wind when solving for atmospheric phenomena. Without signal

direction of arrival and velocity at the sensor, it is impossible to factor in the impact of wind on the effective sound speed. This, in turn, causes inaccuracies when fitting a line to the cross correlograms. Our study was limited by three ground weather atmospheric stations and one wind LIDAR system. For our complex wind environment, this was simply not enough to give us a full understanding of the spatial and possibly temporal variance in wind. The close relationship between the network average and radiosonde temperature ratios suggests that a dense network, like the one used in this study, may have the power to resolve average temperature ratios. However, it is not yet understood if this idea stands should the variance in wind be greater than what was observed in this study. It is important to note that while infrasound sensors were placed over complex topography in this study, topography is static and thus always has the same effect on the acoustic coda. Therefore, differences in topography between the study by Marcillo *et. al* (2014)[3] and this one do not create the observed complexities in temperature ratio. Variable wind speed and direction are the key culprits in creating the complex temperature ratio spread.

## B. Suggestions for Future Research

Measuring signal direction of arrival and velocity at the sensor is a way future studies can aim to better understand complexities resulting from the coda phase delay method. 2D wave gradiometry is a good candidate for this. The method requires closely spaced receivers and can be used to find the back-azimuth and horizontal slowness of an arriving

wave. By focusing on highly correlated coda segments and their back-azimuths, gradiometry could reveal the relationship between phase delays and wave propagation. This could then be directly accounted for in the temperature ratio calculation. Essentially, 2D wave gradiometry can identify the direction of arrival of certain coda elements, allowing for both the vector wind and the scalar temperature fields to be solved for. Understanding the wind and temperature fields would greatly improve temperature ratio calculations. Depending on the site and availability, receivers can be placed in one closely-spaced array or distributed throughout the site in closely-spaced 5-element arrays. For our signal frequency of interest (0.1 – 10 Hz), the gradiometry method only requires sensors to be placed about 10m apart. Thus, there would be no worry about a different source-scatterer-receiver geometry affecting the coda waveforms at such close ranges. The authors plan to experiment with 2D wave gradiometry should a similar experiment be conducted in the future.

**Acknowledgements**

Sandia National Laboratories is a multimission laboratory managed and operated by National Technology and Engineering Solutions of Sandia, LLC., a wholly owned subsidiary of Honeywell International, Inc., for the U.S. Department of Energy's National Nuclear Security Administration under contract DE-NA-0003525.

**REFERENCES**

**1.** Aki, K. and Chouet, B. (**1975**). "Origin of coda waves: Source, attenuation, and scattering effects," J. Geophys. Res. **80**(23), 3322-3342, doi:10.1029/JB080i023p03322

**2.** Blom, P. and Waxler, R. (**2012**). "Impulse propagation in the nocturnal boundary layer: Analysis of the geometric component," J. Acous. Soc. Am. **131**(5), 3680-3690.

**3.** Marcillo, O., Arrowsmith, S, Whitaker, R., Morton, E., and Phillips, W. Scott. (**2014**). "Extracting changes in air temperature using acoustic coda phase delays," J. Acoust. Soc. Am. **136**(4), EL309–EL314.

**4.** Perepelkin, V. G., Kulichkov, S. N., Chunchuzov, I. P., and Kuznetsov, R. D. (**2011**). "On Experience in using the remote acoustic method of partial reflections in studies of the lower troposphere, Izvestiya," Atmos. Oceanic Phys. **47**(1), 1-14.

**5.** Poupinet, G., Ellsworth, W. L., and Frechet, J. (**1984**). "Monitoring velocity variations in the crust using earthquake doublets: An application to the Calaveras Fault, California," J. Geophys. Res. **89**(B7), 5719-5731, doi:10.1029/JB089iB07p05719.

**6.** Ratdomopurbo, A. and Poupinet, G. (**1995**). "Monitoring a temporal change of seismic velocity in a volcano: Application to the 1992 eruption of Mt. Merapi, (Indonesia)," Geophys. Res. Lett. **22**(7), 775-778, doi:10.1029/95GL00302.

198 **7.** Roberts, P. M., Phillips, W. S., and Fehler, M. C. (**1992**). "Development of the
199 active doublet method for measuring small velocity and attenuation changes in
200 solids," J. Acous. Soc. Am. **91**(6), 3291-3302.

201 **8.** Sneider, R. (**2006**). "The theory of coda wave interferometry," Pure Appl. Geophys.
202 **163**(2-3), 455-473.